

TWO DIMENSIONAL NUMERICAL ANALYSIS OF OPERATING AND GEOMETRICAL PARAMETERS EFFECT ON THE FUEL CELL PERFORMANCE

Sajad Rezazadeh¹, Nima Ahmadi², Nader Pourmahmoud¹ Iraj Mirzaee¹

¹CFD Research center, Mechanical Engineering Department, Urmia University, Urmia, Iran

²CFD Research center, Mechanical Engineering Department, Urmia University of Technology, Urmia, Iran

E-mail: sor.memms@gmail.com

ABSTRACT

This article presents the results of a numerical investigation, using a comprehensive two-dimensional, single phase, non-isothermal and parallel flow model of a PEM fuel cell with straight channels. The proposed model is single domain and both of the anode and the cathode humidification were involved in the domain. In this research, the cathode pressure variation effect on the inlet gas composition (water and oxygen), temperature distribution, molar concentration of species and fuel cell performance were investigated. Also for two low cell voltages (which leads to high current densities), the temperature distribution along the cell has been obtained. Additionally, species distribution such as hydrogen (at the anode side), oxygen and water (at the cathode side) and cathode over potential for various cell voltages have been presented with more details. Furthermore in order to geometrically investigation, three cases with different membrane thicknesses were simulated. Similar boundary conditions employed in mentioned geometries. The results showed that the fuel cell with higher membrane thickness has low performance because ion conductivity resistance increases as the membrane thickness grows up. Finally the numerical results of proposed CFD model have been compared with the available experimental data that represent good agreement.

Keywords: PEMFC; Cathode pressure; Temperature distribution; over potential

1. INTRODUCTION

The proton exchange membrane fuel cell (PEMFC) using very thin polymer membrane as electrolyte has been considered as a promising candidate of future power sources, especially for transportation applications and residential power. This type of fuel cell has many important advantages such as high efficiency, clean, quiet, low temperature operation, capable of quick start-up, no liquid electrolyte and simple cell design. However, its performance and cost should be further optimized before this system becomes competitive with the traditional combustion power plants [1-3].

In a fuel cell, fuel (e.g., hydrogen gas) and an oxidant (e.g., oxygen gas from the air) are used to generate electricity, while heat and water are typical products of the fuel cell operation. Extensive research efforts have been devoted to develop realistic simulation models in the past decade. Researchers all over the world are focusing on optimizing the fuel cell system to be cost competitive with currently available energy conversion devices [4]. Many studies have examined various aspects of PEMFC performance as a function of operating conditions (e.g. [5–13]). One of the important tools in the optimization study of fuel cell performance is computational modeling, which can be used to reveal the fundamental phenomena taking place in the fuel cell system [14]. Among the various aspects of PEMFCs that affect cell performance, geometrical parameters play a major role. For example, performance of the fuel cell with smaller shoulder widths is better than those with larger ones [15–18]. N. Pormahmoud et al. investigated the geometrical effect on PEMFC performance [19,20,21]. This article presents the

results of a numerical investigation, using a comprehensive two-dimensional, single phase, non-isothermal and parallel flow model of a PEM fuel cell with straight channels. In this model, major transport phenomena in conventional model of PEMFC, was investigated. Also the effect of pressure and the membrane thickness on cell performance and output cell current density were studied. Finally the numerical results of proposed CFD model are compared with the available experimental data that represent good agreement.

2. MODEL DESCRIPTIONS

2.1 System description

Figure 1 shows a schematic drawing of a single cell of a PEM fuel cell. It is made of two porous electrodes, a polymer electrolyte membrane, two very thin catalyst layers, and two gas distributor plates.

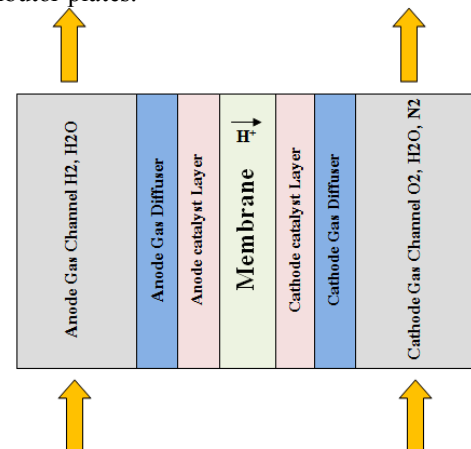


Fig.1 A schematic drawing of a single cell

The channel walls are straight and humidified oxidant gases enter the cathode channel, while humidified fuel enters the anode channel. The conventional single straight channel geometry with computational meshes is shown in figure 2.

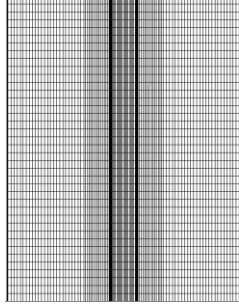


Fig2. X-Y view of the Computational mesh of the domain

2.2 Model Assumptions

The proposed model includes the following assumptions:

- (1) The system operates under a steady-state condition.
- (2) The incoming gas mixtures are considered as an incompressible fluid.
- (3) The fluid flow in the channels is supposed to be laminar because of low velocities gradient and eventually low Reynolds number.
- (4) The membrane is considered impermeable for reactant gases.
- (5) The water in the pores of diffusion layer is separated from the gases in the diffusion layers, i.e. no interaction between the gases and the liquid water exists.
- (6) In the cell, due to electrochemical reaction, the process is non-isothermal; but the walls of the cell and inlet gases have constant temperature (isothermal).

3. GOVERNING EQUATIONS

In this numerical simulation, a single domain model formation was used for the governing equations. These governing equations consist of mass conservation, momentum and species equations, which can be written as:

$$(\nabla \cdot \rho \mathbf{u}) = 0 \quad (1)$$

$$\frac{1}{(\varepsilon^{eff})^2} \nabla \cdot (\rho \mathbf{u} \mathbf{u}) = -\nabla P + \nabla \cdot (\mu \nabla \mathbf{u}) + S_u \quad (2)$$

$$\nabla \cdot (\mathbf{u} C_k) = \nabla \cdot (D_k^{eff} \nabla C_k) + S_k \quad (3)$$

$$\nabla \cdot (\kappa_e^{eff} \nabla \Phi_e) + S_{\Phi} = 0 \quad (4)$$

In Eq.(1) ρ is the density of gas mixture. According to model assumption, mass source and sink term neglected. ε is the effective porosity inside porous mediums, and μ is the viscosity of the gas mixture in the momentum equation is shown as Eq.(2) The momentum source term, S_u , is used to describe Darcy's drag for flow through porous gas diffusion layers and catalyst layers [22] As:

$$S_u = -\frac{\mu}{K} \mathbf{u} \quad (5)$$

K is the gas permeability inside porous mediums. D_k^{eff} In the species equation as shown in Eq. (3), is the effective diffusion coefficient of species k (e.g. hydrogen, oxygen, nitrogen and water vapor) and is defined to describe the effects of porosity in the porous gas diffusion and catalyst layers by the Bruggeman correlation as:

$$D_k^{eff} = (\varepsilon^{eff})^{1.5} D_k \quad (6)$$

Additionally, diffusion coefficient is function of temperature and pressure [23] by next equation:

$$D_k = D_k^o \left(\frac{T}{T_o} \right)^{\frac{3}{2}} \left(\frac{P_o}{P} \right) \quad (7)$$

The charge conservation equation is shown as Eq. (4) and σ is the ionic conductivity in the ion metric phase and has been incorporated by Springer et al. [24] as:

$$\sigma = \exp \left[1268 \left(\frac{1}{303} - \frac{1}{T} \right) \right] \times (0.005139\lambda - 0.00326) \quad (8)$$

Moreover, in recent equation, λ is defined as the number of water molecules per sulfonate group inside the membrane (water content). The water content can be assumed function of water activity, a is defined according to experimental data [25]:

$$\lambda = 0.3 + 6a \left[1 - \tanh(a - 0.5) \right] + 3.9 \sqrt{a} \left[1 + \tanh \left(\frac{a - 0.89}{0.23} \right) \right] \quad (9)$$

Water activity, a is defined by:

$$a = \frac{C_w RT}{P_w^{sat}} \quad (10)$$

The proton conductivity in the catalyst layers by introducing the Bruggeman correlation [26] can be given by:

$$\sigma^{eff} = \varepsilon_m^{1.5} \sigma \quad (11)$$

In recent equation ε_m is the volume fraction of the membrane-phase in the catalyst layer. Local current density in the membrane can be calculated by:

$$I = -\kappa_e \nabla \Phi_e \quad (12)$$

Then the average current density is calculated as follow:

$$I_{ave} = \frac{1}{A} \int_{A_{mem}} I dA \quad (13)$$

Where A is the active area over the MEA.

4. WATER TRANSPORT

Water molecules in PEM fuel cell are transported via electro-osmotic drag due to the properties of polymer electrolyte membrane in addition to the molecular diffusion. H^+ protons transport water molecules through the polymer electrolyte membrane and this transport phenomenon is called electro-osmotic drag. In addition to the molecular diffusion and electro-osmotic drag, water vapor is also produced in the catalyst layers due to the oxygen reduction reaction. Water transport through the polymer electrolyte membrane is defined by:

$$\nabla \cdot (D_{H_2O}^{mem} \nabla C_{H_2O}^{mem}) - \nabla \cdot \left(\frac{n_d}{F} \mathbf{i} \right) = 0 \quad (14)$$

Where n_d and $D_{H_2O}^{mem}$ are defined as the water drag coefficient from anode to cathode and the diffusion coefficient of water in the membrane phase, respectively.

The number of water molecules transported by each hydrogen proton H^+ is called the water drag coefficient. It can be determined from the following equation [25]:

$$n_d = \begin{cases} 1 & \lambda < 9 \\ 0.117\lambda - 0.0544 & \lambda \geq 9 \end{cases} \quad (15)$$

The diffusion coefficient of water in the polymer membrane is dependent on the water content of the membrane and is obtained by the following fits of the experimental expression [27]:

$$D_{H_2O}^{mem} = \begin{cases} 3.1 \times 10^{-7} \lambda \left(e^{0.28\lambda} - 1 \right) e^{\left(\frac{-2346}{T} \right)} \\ 4.17 \times 10^{-8} \lambda \left(1 + 161e^{-\lambda} \right) e^{\left(\frac{-2346}{T} \right)} \end{cases} \quad (16)$$

The terms are therefore related to the transfer current through the solid conductive materials and the membrane. The transfer currents or source terms are non-zero only inside the catalyst layers. The transfer current at anode and cathode can be described by Tafel equations as follows:

$$R_{an} = j_{an}^{ref} \left(\frac{[H_2]}{[H_2]_{ref}} \right)^{\gamma_{an}} \left(e^{\alpha_{an} F \eta_{an} / RT} - e^{-\alpha_{cat} F \eta_{an} / RT} \right) \quad (17)$$

$$R_{cat} = j_{an}^{ref} \left(\frac{[O_2]}{[O_2]_{ref}} \right)^{\gamma_{cat}} \left(-e^{\alpha_{an} F \eta_{cat} / RT} + e^{-\alpha_{cat} F \eta_{cat} / RT} \right) \quad (18)$$

According to the Tafel equation, the current densities in the anode and cathode catalysts can be expressed by the exchange current density, reactant concentration, temperature and over-potentials according to the Tafel equations. Where, the surface over potential is defined as the difference between proton potential and electron potential.

$$\eta_{an} = \varphi_{sol} - \varphi_{mem} \quad (19)$$

$$\eta_{cat} = \varphi_{sol} - \varphi_{mem} - V_{oc} \quad (20)$$

The open circuit potential at the anode is assumed to be zero, while the open circuit potential at the cathode becomes a function of a temperature as:

$$V_{oc} = 0.0025T + 0.2329 \quad (21)$$

The protonic conductivity of membrane is dependent on water content, where σ_m is the ionic conductivity in the ionomeric phase and has been correlated by Springer et al. [24]:

$$\sigma = (0.005139\lambda - 0.00326) \exp \left[1268 \left(\frac{1}{303} - \frac{1}{T} \right) \right] \quad (22)$$

Energy equation given by Eq. (23):

$$\nabla \cdot (\rho \mathbf{u} \mathbf{T}) = \nabla \cdot (\lambda_{eff} \nabla \mathbf{T}) + \mathbf{s}_T \quad (23)$$

Where, λ_{eff} is the effective thermal conductivity, and the source term of the energy equation, \mathbf{s}_T , is defined with the following equation:

$$S_T = I^2 R_{ohm} + h_{reaction} + \eta_a i_a + \eta_c i_c \quad (24)$$

In this equation, R_{ohm} , is the ohmic resistance of the membrane, $h_{reaction}$, is the heat generated thorough the chemical reactions, η_a and η_c , are the anode and cathode over potentials, which are calculated as:

$$R_{ohm} = \frac{t_m}{\sigma_e} \quad (25)$$

Here, t_m is the membrane thickness.

$$\eta_a = \frac{RT}{\alpha_a F} \ln \left[\frac{IP}{j_{0a} P_{O_2}} \right] \quad (26)$$

$$\eta_c = \frac{RT}{\alpha_c F} \ln \left[\frac{IP}{j_{0c} P_{O_2}} \right] \quad (27)$$

Where, α_a and, α_c are the anode and cathode transfer coefficients, P_{O_2} is the partial pressure of hydrogen and oxygen, and, j_0 is the reference exchange current density.

The fuel and oxidant fuel rate \mathbf{u} is given by following equations:

$$\mathbf{u}_{in,a} = \frac{\xi_a I_{ref} A_{mem}}{2C_{H_2,in} F A_{ch}} \quad (28)$$

$$\mathbf{u}_{in,c} = \frac{\xi_c I_{ref} A_{mem}}{4C_{O_2,in} F A_{ch}} \quad (29)$$

In present equation, I_{ref} and ξ are the reference current density and stoichiometric ratio, respectively. ξ is defined as the ratio between the amount supplied and the amount required of the fuel based on the reference current density.

5. NUMERICAL IMPLEMENTATION

As mentioned earlier, a two-dimensional full cell model was numerically simulated to analyze the electrochemical reactions, the transport phenomena of the reactants, and products in the cell. The governing equations were discretized using a finite volume method and solved by a CFD code. Numerical results tests were performed to ensure that the solutions were independent of the grid size. Moreover, the computational domain is divided into about 14000 cells. Operating conditions used in this study are summarized in Table 1.

Table1. Cell operating conditions

| parameter | symbol | value |
|--|----------------|-------|
| Cell temperature (°C) | T_{cell} | 80 |
| Pressure at the anode (atm) | P_a | 3 |
| Relative humidity of inlet fuel | RH_a | 1 |
| Pressure at the cathode (atm) | P_c | 5 |
| Relative humidity of inlet air | RH_c | 1 |
| Anode stoichiometry | ζ_a | 2.8 |
| Cathode stoichiometry | ζ_c | 3 |
| Reference current density (A/cm ²) | I_{ref} | 1 |
| Anode transfer coefficient | α_{an} | 2 |
| Cathode transfer coefficient | α_{cat} | 2 |

The proton transfer in the proton conducting regions and the electron transfer in the electronic conducting regions, determine the potential distribution in a cell. One can notice that, the polymer as an electrolyte in the membrane and catalyst, belongs to proton conducting region. While the catalysts, GDLs and BPs including gas flow channels is regarded as electrode. Important geometrical parameters are listed in Table 2.

Table2. Cell design parameter

| Parameter | value |
|---|--------|
| Cell /electrode length (mm) | 71.12 |
| Gas channel width (mm) | 0.762 |
| GDL thickness (mm) | 0.254 |
| Porosity of anode GDL (ϵ) | 0.4 |
| catalyst layer thickness (mm) | 0.0287 |
| Porosity of catalyst layer (ϵ) | 0.112 |
| Membrane thickness (mm) | 0.23 |

6. RESULTS AND DISCUSSIONS

A series of simulation were carried out on the model from low to high operating current densities. In order to evaluate the validity of the model, numerical simulation results (for conventional model or base case) compared with the

experimental data [28], as shown in figure 3, which there is a favorable agreement between them. The power density curve for the model is illustrated too. As we know, there is a relation between voltage, current density and the power of the fuel cell as $P=V*I$.

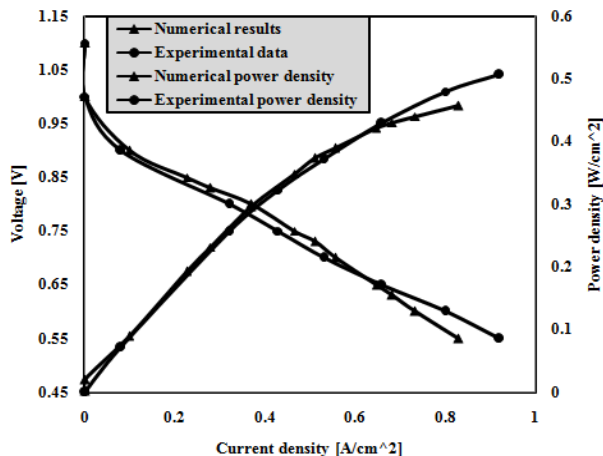


Fig.3 Predicted and experimental cell polarization curves

6.1 Water and oxygen distribution

Figure 4 illustrates the water distribution at the fully humidified anode and cathode side. It is observed that the water molar concentration decreased along the anode side. It was caused by electro-osmotic drag directing from the anode to the cathode. At the anode side, water molecules transfer the H^+ to the cathode side. As the cell voltage decreases (and electrochemical reaction rate increases) this phenomenon takes place faster, so there would be lower hydrogen and water at anode side. On the other hand, the water concentration at the cathode side increased along the cell. It is associated with the fact that the water was formed by electrochemical reaction along the channel and water was transported from anode side by electro-osmotic drag simultaneously. Oxygen mole concentration decreased along the cathode side (Fig.5). Because it reacts with the H^+ that has come from anode side and consequently forms water. So oxygen is consumed and its value decreases along the cell. Decreasing of cell voltage (increasing of current density) accelerates the electrochemical reaction rate and the oxygen consumption (water production). Figure 4 indicates that molar concentration of water at the cathode side layer increases while the cell voltage is decreasing, because the higher current density (lower cell voltage) leads to higher oxygen consumption and so higher water production.

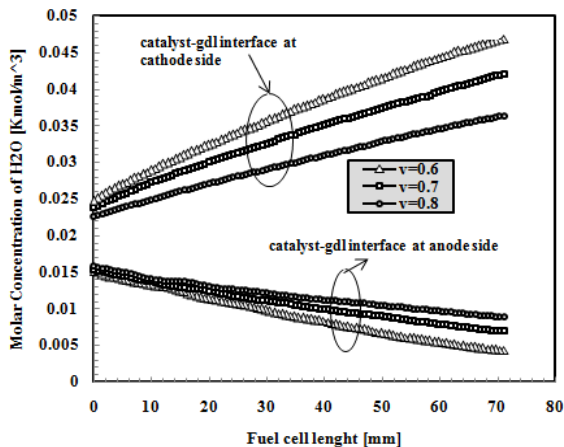


Fig.4 Water mole concentration for different voltages

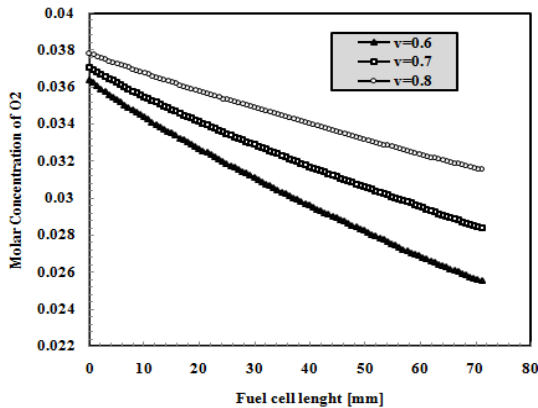


Fig.5 Oxygen mole concentration at the interface of cathode GDL and catalyst layer for different voltages

6.2 Temperature distribution

Temperature distribution is shown in figures 6,7 at the cathode side for two different voltages.

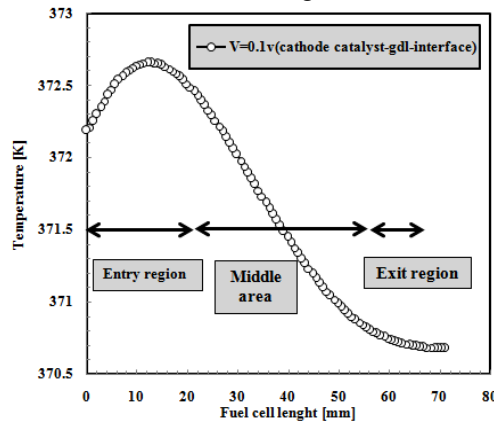


Fig.6 Temperature distribution diagram at the interface of the GDL and the cathode catalyst layer ($V=0.1v$)

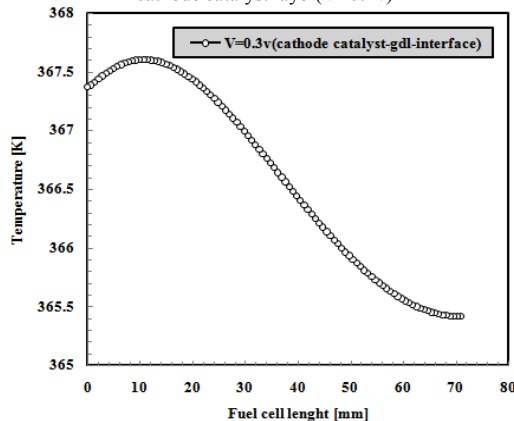


Fig.7 .Temperature distribution diagram at the interface of the GDL and the cathode catalyst layer ($V=0.3v$)

The temperature distribution diagram indicates that temperature value at the entry region of fuel cell is higher than the exit region. It is because of the water production increase along the cathode side and it is obvious that water has important effect on fuel cell heat management and decreasing of temperature.

6.3 Species distribution

6.3.1 Hydrogen distribution

Figure 8 shows the average molar concentration of hydrogen in anode gas channel. CH_2 decrease with decrease of cell potential since the rate of hydrogen oxidation reaction increases. Hydrogen distribution along the middle of anode flow channel, interface of anode flow channel and gas

diffusion layer (GDL) and the interface of anode GDL and catalyst layer has been shown in Figure 9. Approaching to the electrochemical reaction area, the hydrogen amount decreases. Because, all of the hydrogen molecules which are existing in the channel cannot penetrate into the catalyst layer.

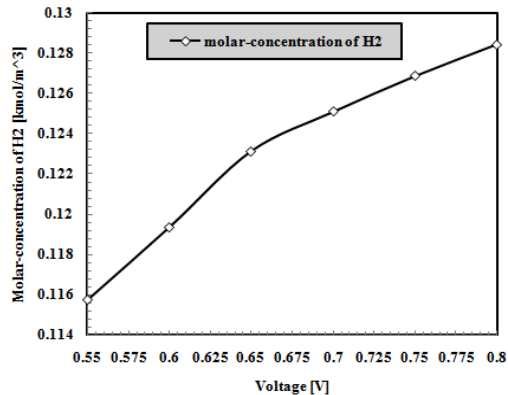


Fig. 8. The averaged molar concentration of gas hydrogen in anode gas channel for different voltages

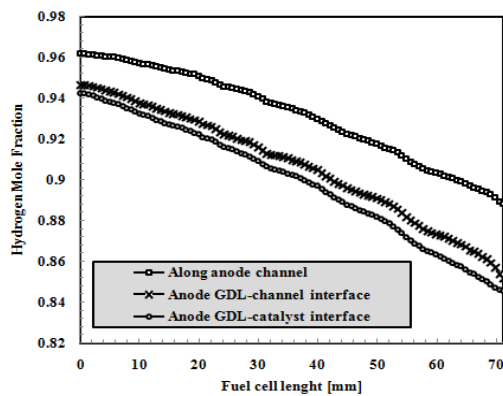


Fig. 9. Mole fraction of hydrogen along the different layers at anode side

6.4 Cathode over potential

At the interface of the membrane and the cathode catalyst layer, the average values of the cathode over potential have been shown for three different voltages (Fig.10). The cathode over potential is affected by the oxygen mole fraction. According to figure5, the oxygen mole fraction is higher in the inlet region than the exit area, which gives rise to higher water production in the exit area. The produced water in the cathode reacting area blocks the holes of the porous GDL, this circumstance reduces diffusion of the oxygen to the reacting area.

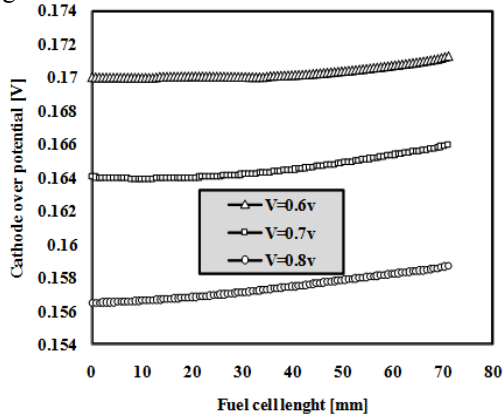


Fig.10. cathode over potential at the interface of the GDL and the cathode catalyst layer

6.5 Effect of pressure

For pressures above 3 atm the composition changes only slightly with the pressure. The polarization curves shown in Figure11 reveal change in the current density amount especially in the low voltage region (0.5-0.3V), when the pressure is changed. This can be attributed to the change in the equilibrium potential that goes along with a decrease in the reactant pressure (Nernst equation). To a much lesser extent, the decrease in the exchange current density with decreasing pressure also contributes to this effect.

Figures 12 and 13 show molar concentration of water and oxygen, at the interface of cathode GDL and cathode catalyst layer for two different cathode pressures, respectively when the cell voltage is 0.7V. According to figures 12, 13, it can be anticipated that the molar concentration of oxygen and water will be increased and decreased respectively, by increasing of cathode pressure. It is clear that cathode pressure has significant effect on incoming cathode side gas stream consist of water and oxygen. Figure15 shows the average molar concentration at the cathode side catalyst layer. The cell voltage is maintained constant at 0.7 in all these cases. Increasing of current density results in increasing of oxygen consumption. Increasing of oxygen molar concentration results in increasing of electrochemical reaction rate at the cathode catalyst layer and temperature distribution too, that is clearly shown in figure16 (at cell voltage 0.7).

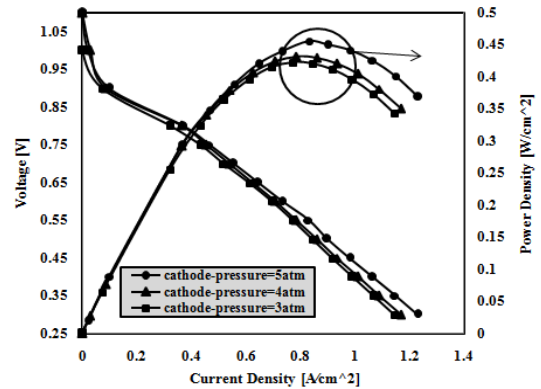


Fig. 11. Cathode pressure effect on cell performance

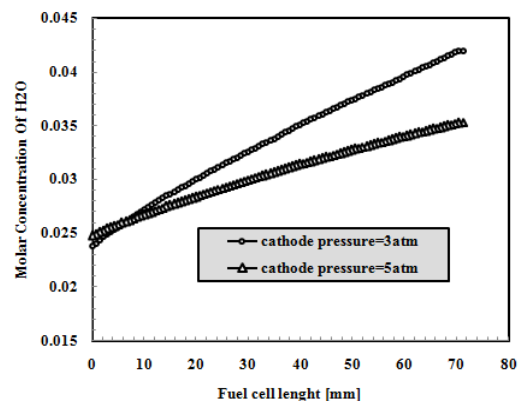


Fig. 12. Molar concentration of water the at interface of cathode GDL and cathode catalyst layer(V=0.7v)

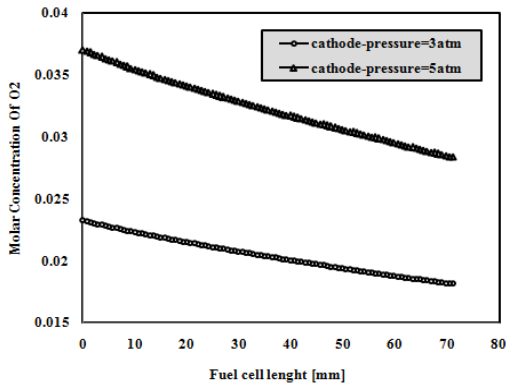


Fig. 13. Molar concentration of oxygen at the interface of cathode GDL and cathode catalyst layer($V=0.7v$)

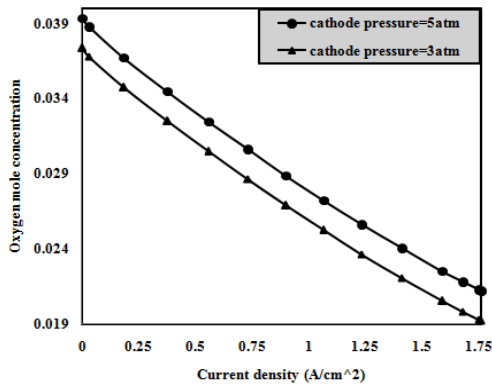


Fig. 14. The average molar concentration at the cathode side catalyst layer

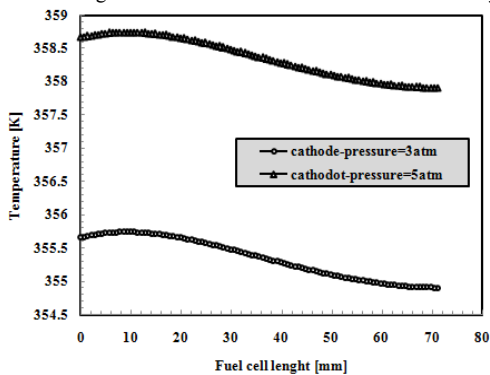


Fig. 15. Temperature distribution diagram at the interface of the GDL and the cathode catalyst layer ($V=0.7v$)

6.6 Effect of membrane thickness

The effect of membrane thickness on the fuel cell potential and current density is displayed in figure 16. As the membrane thickness decreases, the H^+ path to reach the electrochemical reaction area (cathode catalyst layer) decreases. It means that the ion conductivity resistance (ohmic loss) decreases. In this way, H^+ reaches the cathode catalyst layer sooner and combines with the oxygen faster and forms the water further (figures 17, 18, 19). Figure 18 indicates that in the case with thicker membrane, the oxygen consumption and consequently water formation is lower. It is clear that in fuel cell with high reaction rate (oxygen and water combination rate), the current density and performance is better. So it can be resulted that the case with lower membrane thickness has better performance. Figure 20 indicates the current density distribution of two proposed model (case 1: thinner membrane & case 2: thicker membrane). As it discussed before, the performance of fuel cell with thicker membrane (case 2) is lower than the case with thinner membrane (case 1). It can be obtained that the protonic conductivity of case 1 should be better than case 2,

because it can transfer the H^+ easier and faster than case 2 which has been shown in figure 22. As mentioned before, the amount of water production in case 1 is higher than case 2. So the case 1 consumes more oxygen and results in anoxia phenomenon. Additional water produced in case 1 can block the holes of cathode catalyst layer. This means that cathode over potential should be higher in case 1 (Fig. 21). While the water magnitude in case 2 is lower than case 1, then the heat transfer of case 2 will be weaker than case 1, which leads to higher temperature in case 2 (Fig. 23). According to Eq. (10) the anode water activity has inverse relation with saturated pressure. As it is clear, Saturation pressure is only a function of temperature. So the higher temperature leads to lower water activity, which has been shown in figure 24.

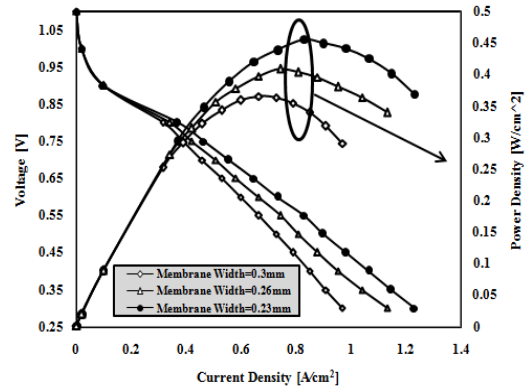


Fig. 16. Effect of membrane thickness on fuel cell performance

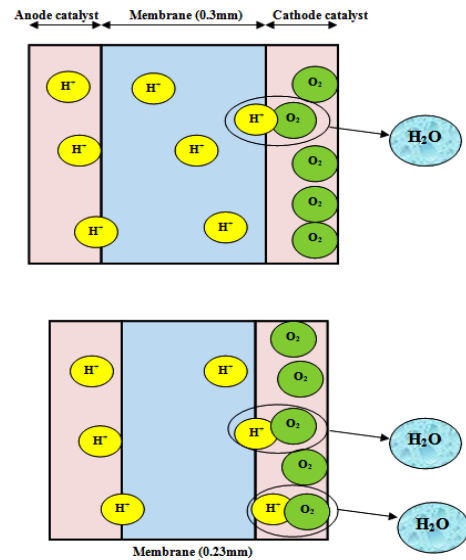


Fig. 17. Schematic of H^+ path to the cathode catalyst layer

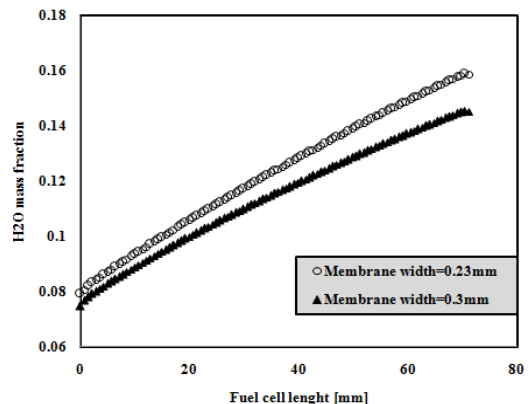


Fig. 18. H_2O mass fraction for $V=0.6 [V]$

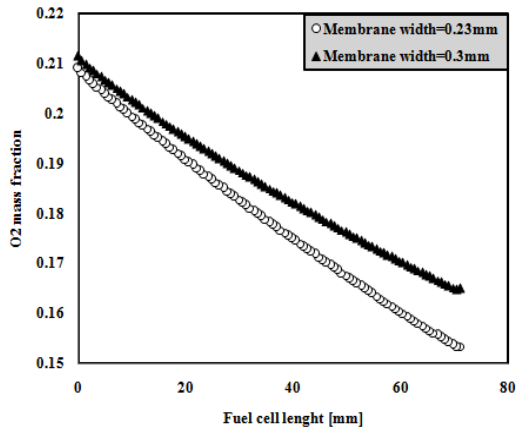


Fig.19. O₂ mass fraction for V=0.6 [V]

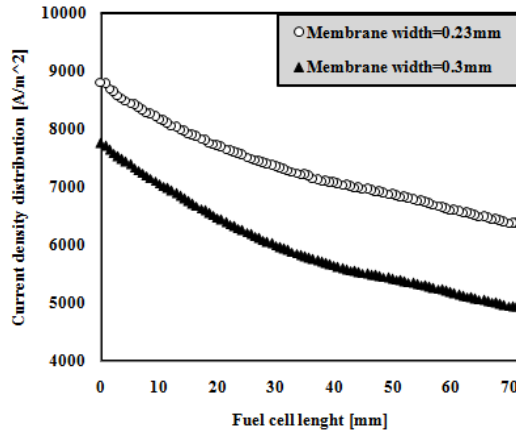


Fig.20. Current density for V=0.6 [V]

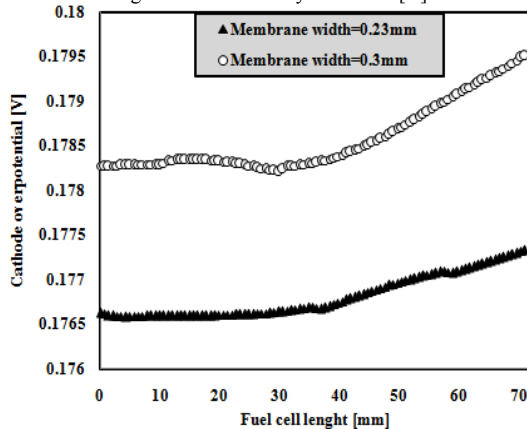


Fig.21. Cathode overpotential for V=0.6 [V]

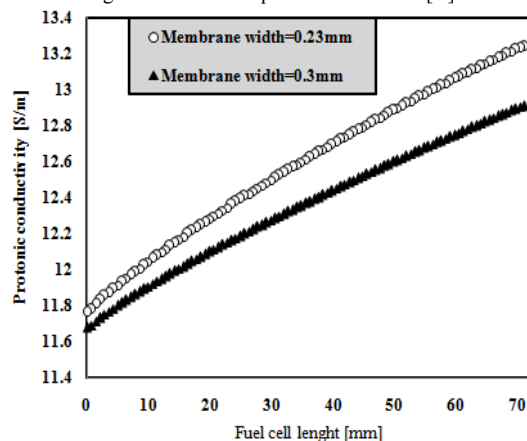


Fig.22. Protonic conductivity for V=0.6 [V]

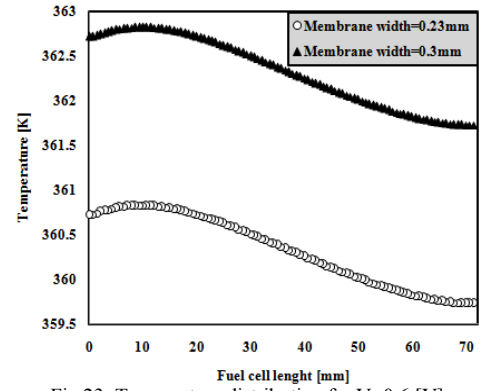


Fig.23. Temperature distribution for V=0.6 [V]

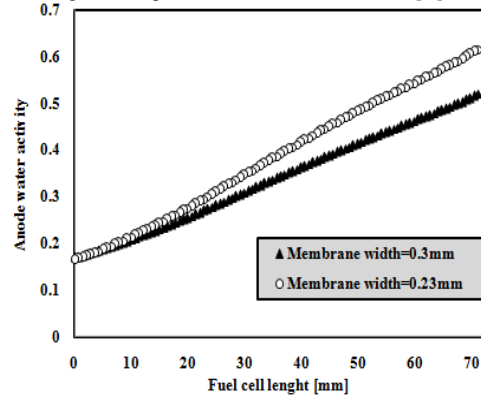


Fig.24. Anode water activity for V=0.6 [V]

7. CONCLUSION

In this article a two dimensional computational fluid dynamics model of a Proton Exchange Membrane Fuel Cell (PEMFC) with straight flow channels has been simulated. Temperature distribution diagram for two low voltages, species distribution such as hydrogen, oxygen and water for different operating voltages and along various interface layers have been presented and discussed with more details. The temperature value at the entry region of fuel cell is higher than the exit region. It is because of the water production increase (due to oxygen consumption which results in water formation) along the cathode side and it is obvious that water has important effect on fuel cell heat management and decreasing of temperature. It is obtained that the cathode over potential is affected by the oxygen mole fraction. As mentioned before the oxygen value is more in the inlet region than the exit area, which gives rise to higher water production in the exit area. The produced water in the cathode reacting area blocks the holes of the porous GDL, this circumstance reduces diffusion of the oxygen to the reacting area. The operating pressure affects numerous parameter that are important for the fuel cell operation. Meanwhile cathode pressure variation effect on the inlet gas composition (water and oxygen), temperature distribution, and molar concentration of species and fuel cell performance have been numerically investigated. On the other hand three geometries with different membrane thickness which have similar boundary conditions have been simulated. As mentioned before ion conductivity resistance decreases as the membrane thickness decreases. As the membrane thickness decreases, the H⁺ path to the electrochemical reaction area (cathode catalyst layer) decreases. It means that the ion conductivity resistance (ohmic loss) decreases. In this way, H⁺ reaches the cathode catalyst layer sooner and combines with the oxygen faster and forms the water further. So it can

be resulted that the case with lower membrane thickness has better performance.

7. REFERENCES

1. A. Kazim, H.T. Liu, P. Forges., "Modeling of performance of PEMFC with conventional and interdigitated flow fields" *Journal of Applied Electrochem.* Vol.29, pp.1409–1416, 1999.
2. T.V. Nguyen., "Modeling two-phase flow in the porous electrodes of proton exchange membrane fuel cells using the interdigitated flow fields," Presented at the 195th Meeting of Electrochemical Society, 4–7 May Seattle, 1999.
3. D.L. Wood, J.S. Yi, T.V. Nguyen, "Effect of direct liquid water injection and interdigitated flow field on the performance of proton exchange membrane fuel cells," *Journal of Appl.Electrochem.* Vol.43, pp.3795–3809, 1998.
4. M. Grujicic, K.M. Chittajallu, "Design and optimization of polymer electrolyte membrane (PEM) fuel cells," *Applied Surface Science*, Vol.227, pp.56–72, 2004.
5. Xing et al., "Optimization of assembly clamping pressure on performance of proton-exchange membrane fuel cells," *Journal of Power Sources*, Vol.195, pp.62-68, 2010.
6. Chang et al., "Effect of clamping pressure on the performance on a PEM fuel cell," *Journal of Power Sources*, Vol.166, pp. 149-154 ,2007.
7. Y.W. Rho, O.A. Velez, S. Srinivasan, Y.T. Kho., "Mass transport in proton exchange membrane fuel cells using O₂/H₂, O₂/Ar, and O₂/N₂ mixtures", *Journal of Electrochem Society*, Vol.141, 3838,1994.
8. J.C. Amphlett, R.M. Baumert, R.F. Mann, B.A. Peppley, P.R.Roberge, T.J. Harris, "Performance modeling of the Ballard Mark IV solid polymer electrolyte fuel cell," *Journal of Electrochem. Society*, Vol.9, pp.142-150, 1995.
9. R. Mosdale, S. Srinivasan, "Analysis of performance and of water management in proton exchange membrane fuel cells", *Electrochem. Acta*, Vol.40, pp.413-421, 1995.
10. H.-F. Oetjen, V.M. Schmidt, U. Stimming, F. Trila, "Performance data of a proton exchange membrane fuel cell using H₂/Co as fuel gas", *Journal of Electrochem Society*, Vol.143, pp.3838-3845, 1996.
11. F.N. Büchi, D. Srinivasan, "Operating Proton Exchange Membrane Fuel Cells without External Humidification of the Reactant Gases" *Journal of Electrochem Society*, Vol.144, pp.2767-2777, 1997.
12. F.A. Uribe, S. Gottesfeld, T.A. Zawodzinski, "Effect of ammonia as potential fuel impurity on proton exchange membrane fuel cell performance". *Journal of Electrochem Society*, Vol.149, pp.293-305, 2002.
13. E.A. Ticianelli, C.R. Derouin, S. Srinivasan, "Localization of platinum in low catalyst loading electrodes to attain high power densities in SPE fuel cells". *Journal of Electroanal Chemistry*, pp.251, 275, 1988.
14. K.Z. Yao, K. Karan, K.B. McAuley, P. Oosthuizen, B. Peppley, T. Xie, "A review of mathematical models for hydrogen and direct methanol polymer electrolyte membrane fuel cells", *Fuel Cells* 4 (1/2) , pp3–29, 2004.
15. D. Natarajan, T.V. Nguyen, "A two-dimensional, two-phase, multi component, transient model for the cathode of a proton exchange membrane fuel cell using conventional gas distributors", *Journal of Electrochem Society*, Vol.148, No.12, pp. A1324–A1335, 2001.
16. [16]G. Lin, T.V. Nguyen, "A two-dimensional two-phase model of a PEM fuel cell", *Journal of Electrochem Society*, Vol.153, No.2, pp.A372–A382, 2006.
17. K.W. Lum, J.J. McGuirk, "Three-dimensional model of a complete polymer electrolyte membrane fuel cell – model

formulation, validation and parametric studies", *Journal of Power Source*, Vol.143, pp.103–124, 2005.

18. D.H. Ahmed, H.J. Sung, "Effects of channel geometrical configuration and shoulder width on PEMFC performance"., *Journal of Power Source*, Vol.162 ,pp. 327–339, 2006.
19. S.Majidifar, I.Mirzaei, S.Rezazadeh, P.Mohajeri, H.Oryani, "Effect of Gas Channel Geometry on Performance of PEM Fuel Cells", *Australian Journal of Basic and Applied Sciences*, Vol.5, No.5, pp.943-954, 2011.
20. N.Pourmahmoud, S.Rezazadeh, I.Mirzaee, V .Heidarpoor, "Three-dimensional numerical analysis of proton exchange membrane fuel cell", *Journal of Mechanical Science and Technology*, Vol.25 ,No.10 ,pp. 2665-2673, 2011.
21. N. Pourmahmoud, S. Rezazadeh, I. Mirzaee, S. Motaleb , "A computational study of a three-dimensional proton exchange membrane fuel cell (PEMFC) with conventional and deflected membrane electrode assembly", *Journal of Mechanical Science and Technology* . Vol.26 ,No.9, pp.2959-2968, 2012.
22. V. Garau, H. Liu, and S. Kakac, *AIChE Journal*, Vol.44, No.11, pp.2410-2422, 1998.
23. R. B. Bird, W. E. Stewart and E. N. Lightfoot, *Transport phenomena* (John Wiley & Sons, Inc, 1960).
24. T. E. Springer, T. A. Zawodzinski, and S. Gottesfeld, "Polymer electrolyte fuel cell", *Journal of Electrochem Society*, Vol.138, No. 8 pp.2334-2342, 1991.
25. A.A. Kuklikovsky, *J. Electrochem. Soc.* Vol.150, No.11, pp. 1432-1439, 2003.
26. R.E.Meredith and C.W.Tobias, "Advances in Electrochemistry and Electrochemical Engineering 2", Tobias, (C.W.Tobias, ed., Interscience Publishers, New York, 1960).
27. S.W. Yeo and A. Eisenberg, *Journal of applied Polymer Science*, 21, pp.875, 1997.
28. E. A. Ticianelli, C. R. Derouin, and S. Srinivasan, *Journal of Electroanal Society*, pp.251- 275, 1988.

NOMENCLATURES

| | |
|----------------------|--|
| a | Water activity |
| C | Molar concentration (mol/m ³) |
| D | Mass diffusion coefficient (m ² /s) |
| F | Faraday constant (C/mol) |
| I | Local current density (A/m ²) |
| J | Exchange current density (A/m ²) |
| K | Permeability (m ²) |
| M | Molecular weight (kg/mol) |
| n_d | Electro-osmotic drag coefficient |
| P | Pressure (Pa) |
| R | Universal gas constant (J/mol-K) |
| T | Temperature (K) |
| t | Thickness |
| \vec{u} | Velocity vector |
| V_{cell} | Cell voltage |
| V_{oc} | Open-circuit voltage |
| W | Width |
| X | Mole fraction |
| Greek letters | |
| α | Water transfer coefficient |
| ε^{eff} | Effective porosity |
| ρ | Density (kg/m ³) |
| ϕ_e | Electrolyte phase potential (v) |
| μ | Viscosity (kg/m-s) |
| σ_e | Membrane conductivity (1/ohm-m) |
| λ | Water content in the membrane |
| ζ | Stoichiometric ratio |
| η | Over potential (v) |